Journal Name

ARTICLE TYPE

Cite this: DOI: 00.0000/xxxxxxxxxx

Screening of Hydrogen Bonding Interactions by a Single Layer Graphene

Babu Gaire,[a†] Saranshu Singla,[a†] and Ali Dhinojwala[a*]

Received Date
Accepted Date

DOI: 00.0000/xxxxxxxxxx

A single layer of graphene when transferred to a solid substrate has the ability to screen or transmit interactions from the underlying substrate, which has direct consequences in applications of this 2D material to flexible electronics and sensors. Previous reports using a multitude of techniques present contradictory views on graphene's ability to screen or transmit van der Waals (vdW) and polar interactions. In the present study, we use interface-sensitive spectroscopy to demonstrate that a single layer graphene is opaque to hydrogen bonding interactions (a subset of acid-base interactions), answering a question that has remained unresolved for a decade. Similar frequency shifts of sapphire hydroxyl (OH) for graphene-coated sapphire in contact with air and polydimethylsiloxane (PDMS) demonstrate the insensitivity of sapphire OH to PDMS. The screening ability of graphene is also evident in the smaller magnitude of this frequency shift for graphene-coated sapphire in comparison to that for bare sapphire. The screening of acid-base interactions by a single layer graphene results in the significant reduction of adhesion hysteresis for PDMS lens on graphene-coated substrates (sapphire and silicon wafer, SiO_2/Si) than bare substrates. Our results have implications in the use of PDMS stamps to transfer graphene to other substrates eliminating the need for a wet-transfer process.

1 Introduction

Graphene, a single-atom-thick sheet of carbon atoms arranged in a hexagonal lattice, is a fascinating material for understanding the physics of two-dimensional (2D) materials and for use in many technological applications.[1,2] Its unique 2D structure, high surface area, optical transparency, and unprecedented electrical, mechanical, and thermal properties make it an attractive material for fabricating transparent, flexible electronics and sensors.[3,4] The use of graphene, the thinnest known material (0.34 nm), as a conformal coating opens up interesting pathways for surface modification of materials. For instance, addition of a graphene layer on copper (Cu) is known to prevent its atmospheric oxidation.[5] Additionally, in most practical applications, graphene is typically supported on an underlying substrate. Thus, the question on how the substrate supporting the graphene layer influences the interactions of graphene with other media has been of significant interest in the past decade.

A technique that has been widely employed in the literature to determine the transparency of graphene (i.e. the extent to which graphene influences interactions between the underlying substrate and media on other side) is contact angle measurements with water and other liquids. However, results from studies utilizing the same approach present controversial ideas on transparency of graphene. For instance, while the first report by Rafiee *et al.* suggested complete wetting transparency of graphene for substrates interacting primarily via van der Waals (vdW) interactions,[6] later work by several researchers suggested partial wetting transparency to complete wetting opacity.[7–11] The transparency of graphene still remains an unresolved topic as Belyaeva *et al.* recently showed complete transparency of graphene to vdW and polar interactions,[12] while Du *et al.* reported only 20% transmission of polar interactions.[13] The controversy over graphene's transparency also prevails in studies utilizing other techniques including atomic force microscopy (AFM) and electron backscatter diffraction (EBSD).[14–17] Tsoi *et al.* inferred complete screening of vdW interactions by a single layer graphene and molybdenum disulfide.[14] However, Chiou *et al.* reported different Hamaker constants on free and supported graphene layers (derived using bimodal AFM) signifying an influence of the underlying substrate.[15] Therefore, more direct spectroscopic approaches would aid in determining the ability of graphene to shield vdW and polar interactions.

[a] *School of Polymer Science and Polymer Engineering, University of Akron, Akron OH 44325*

† These authors contributed equally to this work.

∗ Corresponding Author, Email: ali4@uakron.edu.

Recently, x-ray techniques including x-ray photoelectron spectroscopy (XPS) and x-ray photon correlation spectroscopy (XPCS) have been utilized to understand how the addition of graphene on an underlying substrate influences adsorption.[18–20] Presel *et al.* employed combined experimental XPS and theoretical approach to study adsorption of carbon monoxide (CO) and argon (Ar) and concluded 50% transmission of vdW interactions.[18] In another study, adsorption of water was found to be fully dominated by water-substrate interactions.[19] Additionally, surface-sensitive non-linear spectroscopies, second harmonic generation (SHG) and sum frequency generation (SFG), have been employed to provide insights into graphene's ability to screen or transmit interactions.[21–28] SHG results with water and SFG results with polystyrene on bare and graphene-coated silica suggest partial to complete opacity of graphene towards intermolecular interactions.[22,24,28] Similar conclusions can be derived from structure of ionic liquids on bare and graphene-coated CaF_2 and BaF_2 substrates, and water structure on bare and graphene-coated sapphire.[21,25,26] However, adsorption of 1-hexanol from cyclohexane on bare and graphene coated alumina,[23] and water structure on bare and graphene-coated CaF_2 and silica substrates indicated negligible effect of the graphene layer.[27] All these studies indirectly analyze the effect of graphene by comparing spectral signatures across bare and graphene-coated substrates. However, the strong dependence of SFG signals on orientation could influence the conclusions derived thereby necessitating the need for a direct molecular probe for resolving this ongoing debate over transparency of graphene.

Spectroscopic shifts, originally proposed by Badger and Bauer, offer a unique way to determine the nature and strength of intermolecular interactions.[29–35] Kurian *et al.* and Wilson *et al.* combined this concept with surface-sensitive SFG to examine interfacial interactions between hydroxylated sapphire and various non-polar/polar liquids and polymers.[36,37] The frequency shift ($\Delta\nu$) of sapphire surface hydroxyls (OH) provided a direct measure of interaction strength. Weak vdW interactions shifted the sapphire OH peak by only 20-30 cm^{-1} with respect to its position in air, while strong acid-base interactions (a broad term encompassing hydrogen bonding, donor-acceptor, and electrophile-nucleophile interactions) shifted the sapphire OH by as much as 120 cm^{-1}. The interaction energy calculated using the observed frequency shifts correlated well with that calculated using Drago-Wayland coefficients signifying the validity of this approach.[36–38] Further, this concept successfully predicted the preferential surface segregation of strongly interacting component from binary liquid mixtures, polymer blends, and polymer solutions, consistent with experimental and simulation results.[39–42] The differences in the frequency shift of sapphire OH peak in contact with another media with or without graphene layer could provide direct evidence of graphene's transparency towards vdW and polar interactions.

In the present study, we investigate the ability of graphene to screen acid-base interactions between polydimethylsiloxane (PDMS) and hydroxylated sapphire (and silicon wafer, SiO_2/Si) using a combination of adhesion and interface-sensitive spectroscopy measurements. PDMS-sapphire and PDMS-SiO_2/Si were chosen because it is well known that acid-base interactions between weakly basic siloxane (Si-O-Si) groups of PDMS and acidic OH groups of sapphire (or SiO_2/Si) result in a significantly high adhesion hysteresis (i.e. work done in separating the two surfaces from adhesive contact is larger than the work done in bringing the two surfaces in contact).[43,44] A comparison of the differences between bare and graphene-coated substrate in terms of adhesion behavior and sapphire OH peak shifts would provide a clear understanding of graphene's transparency. Our adhesion results indicate a significant reduction in adhesion hysteresis for graphene-coated substrates, indicating the screening of acid-base interactions by a single layer of graphene. Similar sapphire OH frequency shifts for graphene-coated sapphire in contact with both air and PDMS indicate the insensitivity of sapphire OH to PDMS. Additionally, the relatively small frequency shift of sapphire OH in contact with PDMS for graphene-coated sapphire as compared to bare sapphire further corroborates the opaqueness of graphene to acid-base interactions of the underlying substrate. Our results would benefit the scientific community aiming to understand transparency of graphene and also provide an interesting avenue to quantify PDMS-graphene adhesive interactions crucial for realizing large-scale roll-to-roll transfer of graphene using PDMS stamp.[45–49]

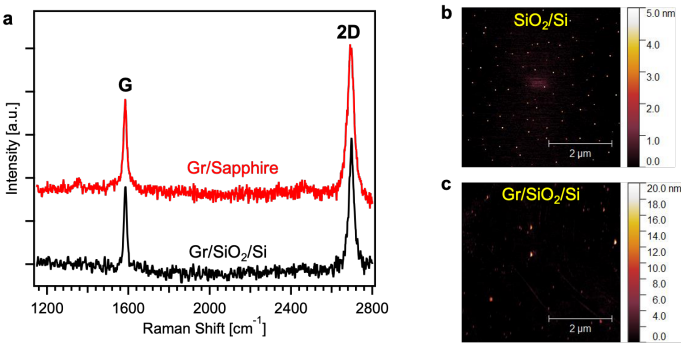

Fig. 1 (a) Representative Raman spectra of the graphene layer transferred onto SiO_2/Si and sapphire substrates. Multiple spots on the same sample are inspected to check for spot-by-spot variance. An intensity ratio of $>$1.5 for 2D (2695 cm^{-1}) and G (1585 cm^{-1}) peaks along with a negligible D (1350 cm^{-1}) peak indicates that the transferred graphene is of good quality with minimal defects. (b) and (c) AFM topographic images of the bare and graphene-coated SiO_2/Si substrates, respectively. Scale bar: 2 μm.

2 Results

2.1 Graphene Characterization

We determine the quality of our monolayer graphene transferred onto SiO_2/Si and sapphire substrates using Raman spectroscopy in order to ensure that the transparency of our graphene is not influenced by defects.[17,50] Figure 1a shows the representative Raman spectra of graphene layer transferred onto SiO_2/Si and sapphire substrates, which show prominent peaks at 1585 cm^{-1} and 2695 cm^{-1} known as the G and 2D peaks, respectively.[51] Absence of D peak at $\sim$1350 cm^{-1} indicates that the transferred graphene is defect free. The calculated ratio of intensity for 2D and G peaks ($I_{2D}/I_G>1.5$) along with a narrow full width half maxima (FWHM) of 2D peak confirms the presence of a good quality monolayer graphene. We further evaluate the conformality of graphene to the underlying substrates by collecting AFM topographical images of bare and graphene-coated substrates (Figure 1b, c). The AFM image of graphene-coated SiO_2/Si appears very similar to that of the underlying SiO_2/Si substrate with very few wrinkles caused by the wet transfer technique.[51] The calculated root mean square (RMS) roughness values for graphene(Gr)/SiO_2/Si (77$\pm$15 pm) and SiO_2/Si (59$\pm$6 pm) are similar, providing evidence of conformal contact between graphene monolayer and the underlying silicon wafer. Similar roughness values are observed for bare (63$\pm$9 pm) and graphene-coated (82$\pm$15 pm) sapphire substrates (Figure S1, †ESI).

2.2 Adhesion Measurements

We perform adhesion measurements using a custom-designed JKR setup (Figure 2a),[52,53] where a soft elastomeric PDMS lens is brought in contact with bare (or graphene-coated) substrates. After loading the lens to a maximum preload of 1 mN and equilibrating for 3 min, the PDMS lens is retracted at a constant speed of 60 nm/s until pull-off event occurs before complete detachment. During both loading and unloading, force (F) and contact area are recorded simultaneously. The loading curve is fit with Equation 1 to calculate W_a from loading. Since it is difficult to obtain a good fit for the unloading data, we use the pull-off force ($F_{pull-off}$) to calculate W_a during unloading using Equation 3. Figure 2b shows the contact radius cube (a^3) vs. load (F) plot for 1.9 MPa PDMS lens on Gr/SiO_2/Si (pink circles) and bare SiO_2/Si (black triangles) during loading (or approach) and unloading (or retraction). For Gr/SiO_2/Si, the unloading curve follows a path similar to loading. However, for bare SiO_2/Si, the unloading curve follows a different path compared to loading indicating significantly larger amount of adhesion hysteresis (i.e., work done in separating the PDMS and SiO_2/Si surfaces is larger than the work done in bringing them in contact). Additionally, the higher strain energy release rate (G, calculated by solving Equation 1 at each data point (Figure S2, †ESI)) from unloading as compared to loading also highlights this large adhesion hysteresis. The moduli of PDMS lenses has a negligible effect on the adhesion behavior as similar results are observed for 0.7 MPa PDMS lenses (Figure S3, †ESI). The adhesion results obtained for 1.9 MPa PDMS lenses on graphene-coated (red circles) and bare sapphire (blue squares) substrates (Figure 2c) are consistent with trends observed with graphene-coated and bare SiO_2/Si.

The W_a values obtained from loading and pull-off data for PDMS lenses tested on bare and graphene-coated SiO_2/Si and sapphire substrates are summarized in Figure 2d. The W_a values obtained from loading for Gr/SiO_2/Si and SiO_2/Si are 46±5 mJ/m^2 and 55±2 mJ/m^2, respectively. Similar W_a values are obtained for uncoated and graphene-coated sapphire substrates. Interestingly, the effect of graphene is more evident in the W_a values obtained from pull-off measurements. For Gr/SiO_2/Si, the W_a obtained from pull-off is 64±2 mJ/m^2, a value not very different from that obtained from loading implying a low adhesion hysteresis. The amount of adhesion hysteresis for Gr/SiO_2/Si (17±4 mJ/m^2) is similar to the inherent hysteresis of PDMS lenses (18±6 mJ/m^2) measured by testing them on octadecyltrichlorosilane (OTS)-coated silicon wafers (Games-Howell test, p-value=0.94, Figure S4, †ESI). However, for SiO_2/Si substrate, the W_a calculated from pull-off is 360±5 mJ/m^2 (~6 times the value obtained from loading) indicating a large adhesion hysteresis, consistent with literature.[43,44] Same is true for bare and graphene-coated sapphire, except for a slightly larger adhesion hysteresis for graphene-coated sapphire than graphene-coated SiO_2/Si. The high adhesion hysteresis observed for bare substrates has been attributed to acid-base interactions between the acidic surface Si-OH (or Al-OH) groups of silicon wafer (or sapphire) and weakly basic siloxane (Si-O-Si) groups of PDMS.[43,44] The low adhesion hysteresis observed for graphene-coated substrates would thus indicate screening of polar acid-base interactions by a single layer graphene.

2.3 Spectroscopic Measurements

To provide direct evidence of graphene's ability to screen acid-base interactions, we use SFG to examine the contact interface between PDMS and graphene-coated (or bare) sapphire. Before bringing PDMS lens in contact, we collect SFG scans for air-Gr/sapphire and air-sapphire (Figure 3a). The air-sapphire SFG spectrum (red circles) in PPP polarization shows a peak at ~3708±3 cm^{-1}, attributed to the O-H stretch vibration of the sapphire surface OHs not participating in any interactions (or referred to as sapphire free OHs).[36,37,39] In contact with graphene, the sapphire OH peak shifts to 3644±7 cm^{-1} (i.e. frequency shift of 65±9 cm^{-1}, which is similar to 56±13 cm^{-1} observed for benzene in contact with sapphire[37,39]) due to interactions between sapphire OHs and graphene. The observed frequency shift is comparable to that reported by Ohto *et al.* for water free OD in contact with graphene at the air-water interface.[54] Part of the sapphire free OH peak persists even when graphene is in contact with sapphire due to either the inability of all sapphire OHs to interact with graphene or incomplete conformal contact. No C-H signatures are observed in the air-Gr/sapphire SFG spectrum confirming a clean graphene surface.

When PDMS lens is brought in contact with graphene-coated sapphire (Figure 3b), we observe s-CH_3 (~2910 cm^{-1}) and as-CH_3 (~2965 cm^{-1}) signatures attributed to PDMS in the C-H vibrational region (2750–3100 cm^{-1}) confirming that we are indeed probing the contact interface.[55] Interestingly, the shifted sapphire OH peak position for graphene-coated sapphire in air (3643±8 cm^{-1}) and in contact with PDMS (3638±4 cm^{-1}) are similar (t-test, p-value=0.22), suggesting that the sapphire OH is not influenced by presence of PDMS (Figure S5, †ESI). Additionally, the relative amplitude (A_q) of sapphire free OH peak (~3708 cm^{-1}) to the shifted sapphire OH peak (~3640 cm^{-1}) does not vary (t-test, p-value=0.40) for graphene-coated sapphire in contact with air (0.25±0.06) and PDMS (0.22±0.06) across multiple repeats. The screening effect of graphene is much more evident when comparisons are made to the PDMS-sapphire contact spectrum, which shows a significantly higher shifted sapphire OH peak (3606±17 cm^{-1}) due to strong acid-base interactions between sapphire OHs and siloxane groups of PDMS.[37,39] The low frequency shift for graphene-coated sapphire (70±5 cm^{-1}) compared to bare sapphire (106±19 cm^{-1}) in contact with PDMS illustrates screening of acid-base interactions between sapphire OHs and Si-O-Si groups of PDMS by monolayer graphene. The relative intensity of s-CH_3 and as-CH_3 peaks of PDMS differs across PDMS-Gr/sapphire and PDMS-sapphire, which could be due to differences in orientation of methyl groups at the two interfaces.

3 Discussion

Our study clearly illustrates that a single layer graphene is sufficient to screen acid-base interactions of the underlying substrate (SiO_2/Si and sapphire), an unresolved topic in the past decade. The screening of acid-base interactions from the underlying substrate by a single layer graphene is evidenced by comparisons of adhesion behavior, especially during unloading, and spectroscopic shifts for bare and graphene-coated substrates. Our experimentally measured W_a between PDMS and graphene deposited on two different substrates (46-59 mJ/m^2) from loading is in agreement with PDMS-graphene W_a reported in literature (41-44 mJ/m^2, calculated using polar and dispersive surface energy components of contacting surfaces derived from contact angle measurements).[47,49] However, similarity in the loading W_a values for bare and graphene-coated substrates makes it challenging to interpret the transparency of graphene from loading behavior. The screening ability of monolayer graphene, especially to acid-base interactions, is more evident from the unloading behavior, i.e., the significant reduction in the acid-base interactions-driven adhesion hysteresis for graphene-coated substrates relative to bare substrates. For instance, the addition of a single layer graphene onto

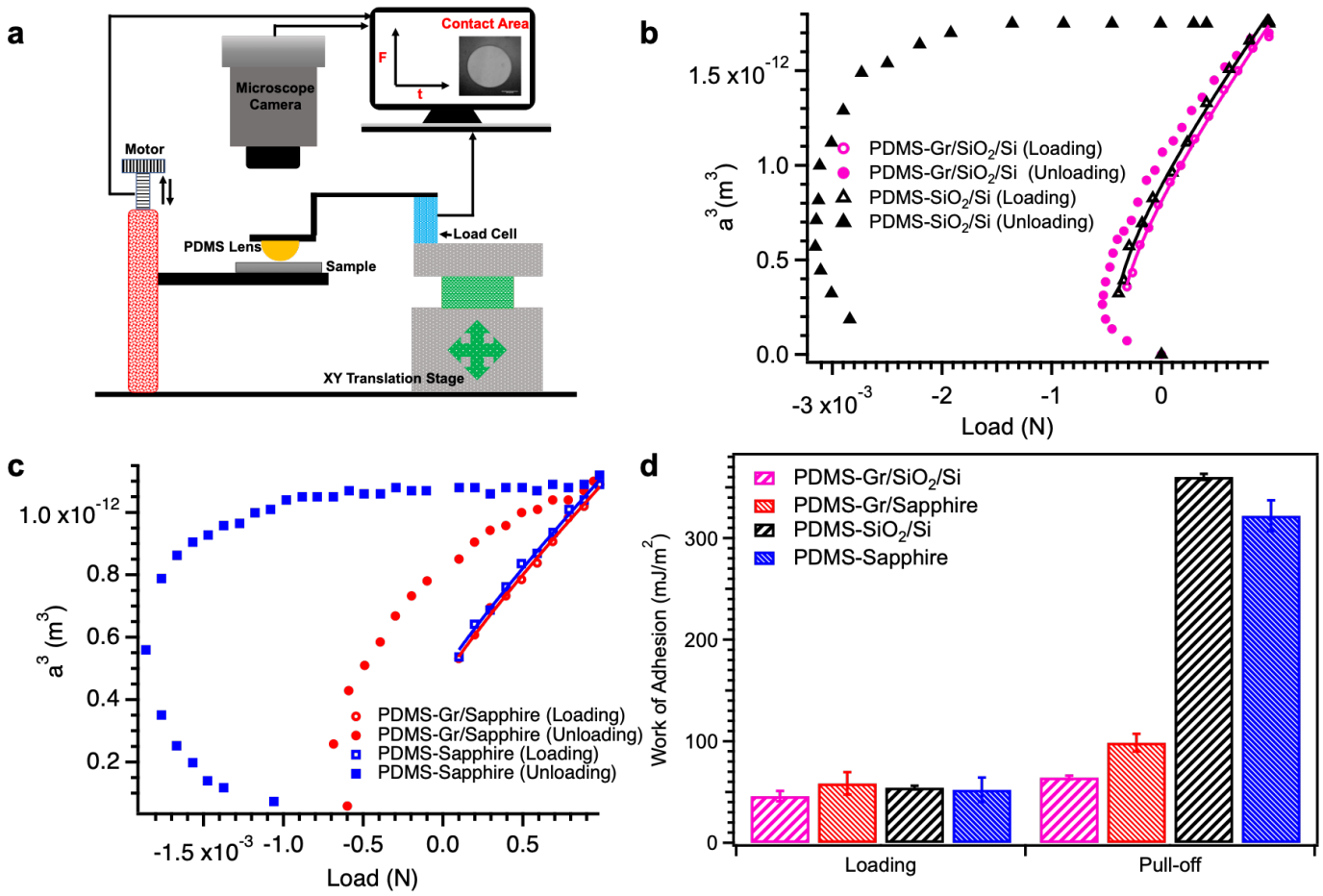

Fig. 2 (a) Schematic of the JKR apparatus used for adhesion experiments. The different components are labeled for clarity. (b) Adhesion measurements during approach (open markers) and retraction (solid markers), where a^3 vs. load (F) data is plotted for 1.9 MPa PDMS lenses on Gr/SiO_2/Si (pink circles) and SiO_2/Si (black triangles) substrates. (c) Adhesion measurements during approach (open markers) and retraction (solid markers), where a^3 vs. load (F) data is plotted for 1.9 MPa PDMS lenses on Gr/sapphire (red circles) and sapphire (blue squares) substrates. (d) Comparison of mean W_a values calculated from loading (by fitting the loading data using Equation 1) and pull-off (calculated using Equation 3) for uncoated and graphene-coated SiO_2/Si and sapphire substrates. Error bars indicate ± 1 standard deviation.

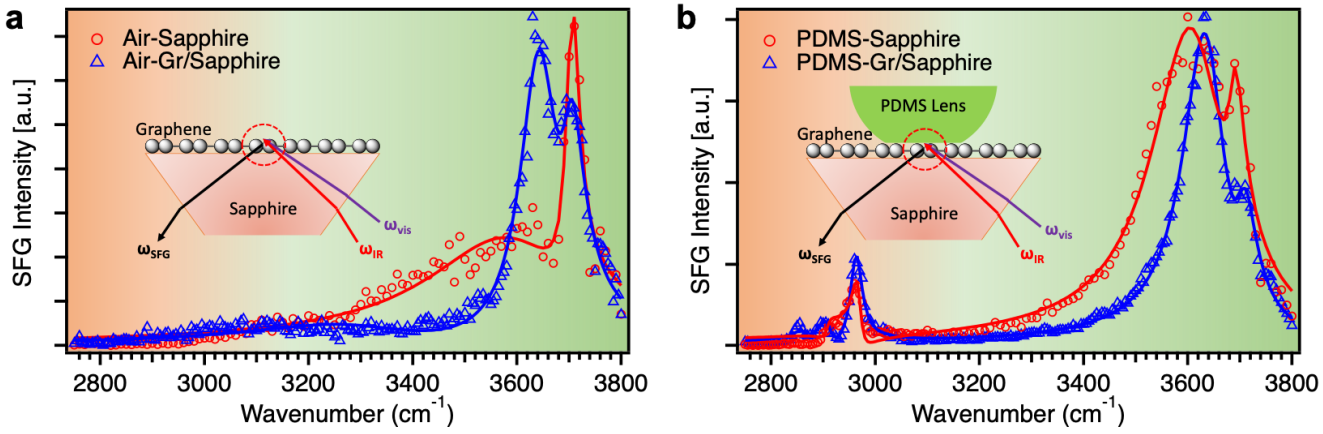

Fig. 3 (a) Representative SFG spectra collected using PPP polarization (P-polarized SFG, P-polarized visible, and P-polarized IR) for air-sapphire (red open circles) and air-Gr/sapphire (blue open triangles). (b) Representative PPP SFG spectra collected for PDMS-sapphire contact (red open circles) and PDMS-Gr/sapphire contact (blue open triangles). The solid lines in both (a) and (b) represent fits obtained by fitting raw data using the Lorentzian equation (Equation 4). Insets show schematics of the experimental geometry used for probing air-Gr/sapphire and PDMS-Gr/sapphire contact interfaces.

SiO_2/Si (or sapphire) substrate reduces adhesion hysteresis from ~300 mJ/m^2 (or ~270 mJ/m^2) to ~20 mJ/m^2 (or ~40 mJ/m^2). This small difference in adhesion hysteresis between graphene-coated SiO_2/Si and sapphire could be due to either a subtle difference between the two underlying substrates (SiO_2/Si and sapphire) or the quality of the graphene coating (wrinkles/folds) transferred on the two substrates.

The large adhesion hysteresis observed for PDMS lenses in contact with oxide surfaces (such as SiO_2 and sapphire) has been reported previously in the literature.[43,44,56,57] Choi *et al.* also showed that the W_a during approach is not different for the adhesion of a PDMS lens to surfaces functionalized with self-assembled monolayers having varying concentrations of polar OH headgroups.[58] However, in their experiments, the adhesion hysteresis increased with an increase in concentration of surface OH groups. PDMS is a hydrophobic polymer with its surface primarily covered by methyl (CH_3) groups.[59] It has been proposed that the PDMS chains near the interface rearrange to allow formation of acid-base interactions between the surface hydroxyl groups and the siloxane repeat units, resulting in high adhesion hysteresis or higher values of strain energy release rate (G) from unloading than loading (Figure S2, †ESI).[43] The addition of a single layer of graphene dramatically reduces adhesion hysteresis, thus providing direct evidence of the disruption of acid-base interactions between the surface Si-OH (or Al-OH) groups and siloxane groups of PDMS. These results are consistent with the hypothesis that during approach, the interactions of PDMS with polar substrates are dominated by vdW interactions.

The influence of strong acid-base interactions between sapphire and PDMS is also manifested in the high frequency shift of sapphire OH for bare sapphire (106±19 cm^{-1}) in contact with PDMS. This shift is significantly higher than the expected frequency shift based on solely vdW interactions (~20-30 cm^{-1}).[36,37] By multiplying the number density of sapphire OH (n) and the enthalpy of PDMS-sapphire interactions (ΔH, calculated using the frequency shift via the Badger-Bauer equation), i.e., $n^*\Delta H$, we calculate the PDMS-sapphire work of adhesion to be 70±12 mJ/m^2.[29,36,39,40,60] The contribution of acid-base interactions to the work of adhesion between PDMS and silica gel has been previously determined by measuring the heat of adsorption using calorimetry (16 mJ/m^2).[58] The W_a calculated by adding the loading W_a (52 mJ/m^2, dominated by vdW interactions) and the acid-base W_a (16 mJ/m^2) is similar to the value estimated from our spectroscopy experiments (70±12 mJ/m^2). However, this W_a is much smaller than the measured W_a value from unloading (~320 mJ/m^2). The experimentally measured high W_a (or G) from unloading is due to the energy dissipated both in stretching of polymer chains at the interface (Lake-Thomas effect) and in breaking acid-base interactions (including hydrogen bonds) during crack propagation (unloading).[58] The energy dissipated in stretching of chains has been shown to be a strong function of velocity.[61] Furthermore, even a velocity as low as 60 nm/s (during unloading cycle) is not sufficient to eliminate the energy dissipated in chain stretching in these experiments.[62] Addition of a single layer of graphene eliminates the contribution of the acid-base interactions (as reflected in the lower frequency shift of sapphire OH for graphene-coated sapphire than bare sapphire) to G, resulting in a low adhesion hysteresis.

The screening of acid-base interactions by a single layer graphene is also discernible from similar frequency shifts of sapphire OH for graphene-coated sapphire in contact with air and PDMS. It is important to underline that our approach used to determine screening ability of graphene is based on a direct spectroscopic method while minimizing the influence of adsorbed contaminants and non-conformality of graphene to the underlying substrate.[6,10,12,13] This approach overcomes the limitations inherent to the widely reported contact angle measurements method (to determine the influence of a single graphene layer). Thus, we can conclude that interactions of graphene with other media are not fully governed by the underlying substrate, especially for substrates interacting via acid-base interactions. Our results have ramifications for applications of graphene as a conductive coating for flexible touch screens, chemical sensors and bio-sensors, and supercapacitors.[46,63–65] The performance of such devices can now be tuned to the interactions between graphene and other media (ions, gases, liquids, proteins) knowing there is little influence of the underlying substrate.

4 Conclusions

In this study, we provide molecular-level evidence of graphene's ability to screen hydrogen bonding interactions (a subset of acid-base interactions) from the underlying substrate, settling a debate that has remained unresolved for a decade. Using interface-sensitive spectroscopy, we demonstrate that a single layer of graphene screens acid-base interactions between oxide surfaces and PDMS. The screening of acid-base interactions is also evident in almost complete elimination of adhesion hysteresis for PDMS on graphene-coated glass and sapphire substrates. Our results have important implications in various technological applications of graphene, including flexible electronics and sensors, where graphene is typically supported on an underlying substrate. In addition, our work highlights that a single layer of graphene can be used to alter surface interactions in adhesion science.

5 Materials and Methods

5.1 Graphene Transfer and Characterization

5.1.1 Wet Transfer of Graphene

A 60 mm × 40 mm sample of chemically vapor deposited (CVD) monolayer graphene grown on Cu foil with a sacrificial poly(methyl methacrylate) (PMMA) coating was purchased from Graphenea Inc. Both silicon wafer (SiO_2/Si) and sapphire substrates were cleaned prior to graphene transfer. The silicon wafers were cleaned using a Piranha solution with 3:7 ratio of 30% hydrogen peroxide (H_2O_2) and concentrated sulfuric acid (H_2SO_4). *Caution should be exercised while handling Piranha solution as the reaction is highly exothermic*. Afterwards, the silicon wafers were rinsed with copious amount of deionized water. The sapphire substrates were cleaned using sequential sonication with toluene, chloroform, acetone, ethanol, and water for at least 1 h each. Just before using, the silicon wafers and sapphire substrates were dried with nitrogen and plasma sterilized for 5 min (Harrick Plasma PDC-32G). Before transferring the monolayer graphene onto the clean silicon wafer (or sapphire plate), the partially removed bottom layer of graphene on Cu foil was etched using a solution of 8:1:1 water, H_2O_2, and concentrated hydrochloric acid (HCl) (following recommendation from Graphenea Inc). Afterwards, the Cu foil was etched using a 0.1 M ammonium persulfate solution for 12 h.[50] Once the Cu foil was completely etched out, the PMMA/graphene film was first rinsed thrice with ultrapure water (Millipore filtration system with a resistivity of 18.2 MΩ·cm) and then transferred onto the clean SiO_2/Si (or sapphire) substrate. The sample was allowed to dry in ambient atmosphere overnight and then vacuum dried at 140°C for 3 h to improve the adhesion between graphene and underlying substrate, and to facilitate PMMA removal using

dissolution with acetone for 12 h.[50] The transferred monolayer graphene on SiO_2/Si (or sapphire) was characterized using Raman spectroscopy and atomic force microscopy (AFM) to check for defects and conformality to the substrate.

5.1.2 Graphene Characterization

Raman spectrum of the graphene transferred on the SiO_2/Si (or sapphire) substrate was obtained using the Renishaw InVia Raman microspectrometer with a 514 nm excitation laser and 50× objective lens to evaluate the quality of graphene. Multiple Raman spectra were collected at different spots on the sample to check for spot-by-spot spectral variance. Additionally, topographic images of the transferred CVD graphene on bare and graphene-coated SiO_2/Si and sapphire substrates were collected using AFM (Bruker Dimension Icon) in the non-contact mode to evaluate the conformality of graphene to the underlying substrate. Multiple spots on different samples were tested in each category to calculate the root mean square (RMS) roughness of bare and graphene-coated substrates.

5.2 Work of Adhesion Measurements

5.2.1 Graphene Surface Cleaning

Since it has been well established that it is hard to get rid of all of PMMA with acetone, the graphene supported on SiO_2/Si (or sapphire) substrate was subjected to thermal annealing at 450°C for at least 1 h under a 10:1 flow of Argon (Ar): Hydrogen (H_2), where the Ar flow rate was set to 1 L/min to remove any remaining contaminants.[10,50] The sample was allowed to cool down to room temperature under an inert atmosphere of Ar. To prevent further adsorption of contaminants, the samples were either immediately used for adhesion measurements or stored in ultrapure water and dried with nitrogen just before adhesion measurements.[10,26,66]

5.2.2 Preparation of PDMS Hemispherical Lenses

Optically transparent hemispherical PDMS lenses of radius 1-2 mm diameter with two different moduli (0.7 and 1.9 MPa) were prepared using the protocol described by Dalvi *et al.*[53] To minimize the influence of uncross-linked PDMS chains on the adhesion results, the PDMS lenses were Soxhlet extracted using toluene for 2 days. Before performing adhesion measurements, the PDMS hemispheres were tested for inherent hysteresis by testing them against a low-surface energy octadecyltrichlorosilane (OTS) monolayer coated silicon wafer (water contact angle ∼110°). The adhesion results with OTS-PDMS demonstrated negligible adhesion hysteresis (difference in the works of adhesion calculated from approach and retraction) due to viscoelasticity (Figure S4, †ESI), thus confirming the removal of any uncrosslinked oligomers.

5.2.3 Adhesion Measurements

A custom-built JKR apparatus, described in previous publications,[52,53] was used to measure the work of adhesion (Figure 2a). Briefly, a PDMS elastomeric lens with a height greater than 700 μm (to avoid the effect of underlying substrate) was adhered on a glass arm and then carefully brought in contact with uncoated and graphene-coated SiO_2/Si (and sapphire) substrates mounted on the load cell with a computer-controlled high resolution Newport picomotor. After confirming contact between the PDMS lens and the sample, the system was loaded to a maximum normal force of 1 mN at a constant loading speed of 60 nm/s. After providing an equilibration time of 3 min, the system was unloaded at a constant velocity of 60 nm/s until the PDMS lens detached from the sample. During loading and unloading, force (F) and contact area were recorded simultaneously with the help of a load cell and an Olympus optical microscope, respectively. A minimum of 3 measurements were performed on each sample and at least 2 different samples were tested to obtain the average work of adhesion from the JKR analysis.

5.2.4 Analysis of Adhesion Data

The experimental force (F) vs. contact radius (a) curve obtained during loading was fit with the JKR equation[67] (Equation 1) using Igor Pro 8, where radius of the PDMS lens (R) is the known parameter (measured using optical microscope) and the thermodynamic work of adhesion (W_a) and the effective elastic modulus (E^*) are unknown parameters. E^* can be calculated using both the modulus (E) and Poisson's ratio (ν) of PDMS elastomer and Gr/substrate, respectively (Equation 2).[68]

$$a^3 = \frac{3R}{4E^*}\left(F + 3W_a\pi R + \sqrt{6W_a\pi RF + (3W_a\pi R)^2}\right) \quad (1)$$

$$\frac{1}{E^*} = \frac{1-\nu_{PDMS}^2}{E_{PDMS}} + \frac{1-\nu_{Gr/Substrate}^2}{E_{Gr/Substrate}} \quad (2)$$

The unloading data was difficult to fit with Equation 1, thus, we use the pull-off force ($F_{pull-off}$) observed during unloading to calculate the W_a using Equation 3. In addition, we plot the strain energy release rate (G) as a function of contact area (Figure S2, †ESI) to express our experimental contact data from the viewpoint of fracture mechanics. The value of G (or W_a) at each point during loading and unloading was obtained by solving the Equation 1 using experimentally measured values of F, R, and a, and value of E^* obtained from fit of loading data .

$$F_{pull-off} = -\frac{3}{2}\pi W_a R \quad (3)$$

5.3 SFG Measurements

5.3.1 Cleaning Procedure

Equilateral sapphire prisms (Meller Optics Inc.) were first baked at 760°C in a quartz tube furnace for at least 3-4 h. Afterwards, the prisms were sonicated (Branson 1510 Utrasonic Cleaner) in a series of solvents including toluene, chloroform, acetone, ethanol, and ultrapure water for at least 1 h per solvent to remove any adsorbed contaminants. The prisms were dried with nitrogen and plasma sterilized for 5 min before either assembling onto the SFG contact cell (using a Teflon spacer) or graphene transfer by the wet transfer approach.[50] The graphene-coated sapphire prism was cleaned via thermal annealing under a 10:1 flow of Ar:H_2 at 450°C for at least 1 h.[10,50] Subsequently, the graphene-coated sapphire prism was cooled to room temperature under Ar atmosphere and immediately assembled onto the contact cell (cleaned by sonication with toluene and chloroform followed by atmospheric plasma treatment for 5 min just before use).

5.3.2 SFG Procedure

SFG spectra were acquired using a picosecond Spectra-Physics laser system, details of which have been described elsewhere.[26,52,55] Briefly, it involves the overlap of a tunable wavelength IR beam (∼3.5 μJ, 1 ps pulse width, and 1 kHz repetition rate) and a fixed 800 nm wavelength visible beam (∼70 μJ, 1 ps pulse width, and 1 kHz repetition rate) at the interface of interest. The resonantly-enhanced SFG signals provide information on the chemical identity and orientation of molecular species at an interface. An incidence angle of 42° (with respect to the sapphire

surface normal) for the IR beam was used to probe the air-sapphire and air-Gr/sapphire interfaces in total internal reflection (TIR) geometry, while an incidence angle of 10° was used to investigate the PDMS-sapphire and PDMS-Gr/sapphire contact interfaces. The incidence angle of the visible laser beam was ∼1.5° lower than that of the IR beam. Additional details on probing the contact interface using SFG can be found in previous studies.[52,55] SFG spectra were collected by scanning in C-H (2750 to 3200 cm^{-1}) and O-H (3100 to 3800 cm^{-1}) vibrational region using PPP polarization (p-polarized SFG, p-polarized visible, and p-polarized IR) because of intense SFG signals in this polarization. The SFG spectra presented in the current study have not been corrected for changes in Fresnel factors as a function of wavenumber[69] and were fit using a Lorentzian function[70]

$$I_{SFG} \propto |\chi_{NR} + \sum \frac{A_q}{\omega_{IR} - \omega_q + i\Gamma_q}|^2, \quad (4)$$

In equation 4, χ_{NR} describes the non-resonant contribution, that does not change with scanning wavenumber (ω_{IR}). A_q, Γ_q, and ω_q are the amplitude strength, damping constant, and resonant frequency of the qth vibrational resonance, respectively.

Conflicts of interest

There are no conflicts to declare.

Acknowledgements

The authors thank Dr. Siddhesh Dalvi and Nityanshu Kumar for helping with the preparation of PDMS lenses. The authors thank Anvay Patil and Austin M. Garner for helping with the AFM experiments and statistical analysis, respectively. The authors also thank Dona Foster and Daniel Maksuta for helpful comments in improving the manuscript. The authors acknowledge funding support from the National Science Foundation (NSF DMR-1610483).

Notes and references

1 A. K. Geim, *Science*, 2009, **324**, 1530–1534.
2 A. K. Geim and K. S. Novoselov, *Nanoscience and Technology: A Collection of Reviews from Nature Journals*, World Scientific, 2010, pp. 11–19.
3 S. Chun, Y. Kim, H. Jung and W. Park, *Appl. Phys. Lett.*, 2014, **105**, 041907.
4 S. Chen, K. Jiang, Z. Lou, D. Chen and G. Shen, *Adv. Mater. Technol.*, 2018, **3**, 1700248.
5 S. Chen, L. Brown, M. Levendorf, W. Cai, S.-Y. Ju, J. Edgeworth, X. Li, C. W. Magnuson, A. Velamakanni, R. D. Piner, J. Kang, J. Park and R. S. Ruoff, *ACS nano*, 2011, **5**, 1321–1327.
6 J. Rafiee, X. Mi, H. Gullapalli, A. V. Thomas, F. Yavari, Y. Shi, P. M. Ajayan and N. A. Koratkar, *Nat. Mater.*, 2012, **11**, 217–222.
7 C.-J. Shih, Q. H. Wang, S. Lin, K.-C. Park, Z. Jin, M. S. Strano and D. Blankschtein, *Phys. Rev. Lett.*, 2012, **109**, 176101.
8 C.-J. Shih, M. S. Strano and D. Blankschtein, *Nat. Mater.*, 2013, **12**, 866–869.
9 R. Raj, S. C. Maroo and E. N. Wang, *Nano lett.*, 2013, **13**, 1509–1515.
10 Z. Li, Y. Wang, A. Kozbial, G. Shenoy, F. Zhou, R. McGinley, P. Ireland, B. Morganstein, A. Kunkel, S. P. Surwade, L. Li and H. Liu, *Nat. Mater.*, 2013, **12**, 925–931.
11 A. Kozbial, Z. Li, C. Conaway, R. McGinley, S. Dhingra, V. Vahdat, F. Zhou, B. D'Urso, H. Liu and L. Li, *Langmuir*, 2014, **30**, 8598–8606.
12 L. A. Belyaeva, P. M. G. van Deursen, K. I. Barbetsea and G. F. Schneider, *Adv. Mater.*, 2018, **30**, 1703274.
13 F. Du, J. Huang, H. Duan, C. Xiong and J. Wang, *Appl. Surf. Sci.*, 2018, **454**, 249–255.
14 S. Tsoi, P. Dev, A. L. Friedman, R. Stine, J. T. Robinson, T. L. Reinecke and P. E. Sheehan, *ACS Nano*, 2014, **8**, 12410–12417.
15 Y.-C. Chiou, T. A. Olukan, M. A. Almahri, H. Apostoleris, C. H. Chiu, C.-Y. Lai, J.-Y. Lu, S. Santos, I. Almansouri and M. Chiesa, *Langmuir*, 2018, **34**, 12335–12343.
16 W. Kong, H. Li, K. Qiao, Y. Kim, K. Lee, Y. Nie, D. Lee, T. Osadchy, R. J. Molnar, D. K. Gaskill, R. L. Myers-Ward, K. M. Daniels, Y. Zhang, S. Sundram, Y. Yu, S. Bae, S. Ranjan, Y. Shao-Horn, K. Cho, A. Ougazzaden, J. C. Grossman and J. Kim, *Nat. Mater.*, 2018, **17**, 999–1004.
17 D. Ghoshal, R. Jain and N. A. Koratkar, *Langmuir*, 2019, **35**, 12306–12316.
18 F. Presel, A. Gijn, E. R. Hernndez, P. Lacovig, S. Lizzit, D. Alfe and A. Baraldi, *ACS nano*, 2019, **13**, 12230–12241.
19 M. H. Bagheri, R. T. Loibl, J. A. Boscoboinik and S. N. Schiffres, *Carbon*, 2019, **155**, 580–586.
20 F. Yang, D. Presto, Y. Pan, K. Liu, L. Zhou, S. Narayanan, Y. Zhu, Z. Peng, M. D. Soucek, M. Tsige and M. D. Foster, *Macromolecules*, 2019, **52**, 5074–5085.
21 S. Baldelli, J. Bao, W. Wu and S.-S. Pei, *Chem. Phys. Lett.*, 2011, **516**, 171–173.
22 J. L. Achtyl, I. V. Vlassiouk, P. F. Fulvio, S. M. Mahurin, S. Dai and F. M. Geiger, *J. Am. Chem. Soc.*, 2013, **135**, 979–981.
23 J. L. Achtyl, I. V. Vlassiouk, S. Dai and F. Geiger, *J. Phys. Chem. C*, 2014, **118**, 17745–17755.
24 J. L. Achtyl, I. V. Vlassiouk, S. P. Surwade, P. F. Fulvio, S. Dai and F. M. Geiger, *J. Phys. Chem. B*, 2014, **118**, 7739–7749.
25 S. Xu, S. Xing, S.-S. Pei and S. Baldelli, *J. Phys. Chem. B*, 2014, **118**, 5203–5210.
26 S. Singla, E. Anim-Danso, A. E. Islam, Y. Ngo, S. S. Kim, R. R. Naik and A. Dhinojwala, *ACS nano*, 2017, **11**, 4899–4906.
27 L. B. Dreier, Z. Liu, A. Narita, M.-J. van Zadel, K. Mllen, K.-J. Tielrooij, E. H. G. Backus and M. Bonn, *J. Phys. Chem. C*, 2019, **123**, 24031–24038.
28 Y. Hong, S. Bao, X. Xiang and X. Wang, *ACS Macro Lett.*, 2020, **9**, 889–894.
29 R. M. Badger and S. H. Bauer, *J. Chem. Phys.*, 1937, **5**, 839–851.
30 M. D. Joesten and R. S. Drago, *J. Am. Chem. Soc.*, 1962, **84**, 3817–3821.
31 K. F. Purcell, J. A. Stikeleather and S. D. Brunk, *J. Am. Chem. Soc.*, 1969, **91**, 4019–4027.
32 C. N. R. Rao, P. C. Dwivedi, H. Ratajczak and W. J. Orville-Thomas, *J. Chem. Soc., Faraday Trans. 2*, 1975, **71**, 955–966.
33 F. M. Fowkes, D. O. Tischler, J. A. Wolfe, L. A. Lannigan, C. M. Ademu-John and M. J. Halliwell, *J. Polym. Sci. A Polym. Chem.*, 1984, **22**, 547–566.
34 F. L. Riddle Jr and F. M. Fowkes, *J. Am. Chem. Soc.*, 1990, **112**, 3259–3264.
35 R. S. Bhatta, P. P. Iyer, A. Dhinojwala and M. Tsige, *Mod. Phys. Lett. B*, 2014, **28**, 1430014.
36 A. Kurian, S. Prasad and A. Dhinojwala, *Langmuir*, 2010, **26**, 17804–17807.
37 M. C. Wilson, S. Singla, A. J. Stefin, S. Kaur, J. V. Brown and A. Dhinojwala, *J. Phys. Chem. C*, 2019, **123**, 18495–18501.

38 R. S. Drago and B. B. Wayland, *J. Am. Chem. Soc.*, 1965, **87**, 3571–3577.

39 S. Singla, M. C. Wilson and A. Dhinojwala, *Phys. Chem. Chem. Phys.*, 2019, **21**, 2513–2518.

40 S. Prasad, H. Zhu, A. Kurian, I. Badge and A. Dhinojwala, *Langmuir*, 2013, **29**, 15727–15731.

41 H. Zhu, N. Dhopatkar and A. Dhinojwala, *ACS Macro Lett.*, 2016, **5**, 45–49.

42 N. Kumar, S. Singla, M. C. Wilson, S. Kaur, S. Bekele, M. Tsige and A. Dhinojwala, *J. Phys. Chem. C*, 2019, **123**, 29729–29738.

43 S. Kim, G. Y. Choi, A. Ulman and C. Fleischer, *Langmuir*, 1997, **13**, 6850–6856.

44 A. Ulman, G.-Y. Choi, Y. Shnidman and W. Zurawsky, *Isr. J. Chem.*, 2000, **40**, 107–121.

45 K. S. Kim, Y. Zhao, H. Jang, S. Y. Lee, J. M. Kim, K. S. Kim, J.-H. Ahn, P. Kim, J.-Y. Choi and B. H. Hong, *Nature*, 2009, **457**, 706–710.

46 S. Bae, H. Kim, Y. Lee, X. Xu, J.-S. Park, Y. Zheng, J. Balakrishnan, T. Lei, H. R. Kim, Y. I. Song, Y.-J. Kim, K. S. Kim, B. Özyilmaz, J.-H. Ahn, B. H. Hong and S. Iijima, *Nat. Nanotechnol.*, 2010, **5**, 574.

47 S. J. Kang, B. Kim, K. S. Kim, Y. Zhao, Z. Chen, G. H. Lee, J. Hone, P. Kim and C. Nuckolls, *Adv. Mater.*, 2011, **23**, 3531–3535.

48 J. Song, F.-Y. Kam, R.-Q. Png, W.-L. Seah, J.-M. Zhuo, G.-K. Lim, P. K. H. Ho and L.-L. Chua, *Nat. Nanotechnol.*, 2013, **8**, 356–362.

49 T. Choi, S. J. Kim, S. Park, T. Y. Hwang, Y. Jeon and B. H. Hong, *Nanoscale*, 2015, **7**, 7138–7142.

50 J. W. Suk, A. Kitt, C. W. Magnuson, Y. Hao, S. Ahmed, J. An, A. K. Swan, B. B. Goldberg and R. S. Ruoff, *ACS Nano*, 2011, **5**, 6916–6924.

51 A. C. Ferrari, J. C. Meyer, V. Scardaci, C. Casiraghi, M. Lazzeri, F. Mauri, S. Piscanec, D. Jiang, K. S. Novoselov, S. Roth and A. K. Geim, *Phys. Rev. Lett.*, 2006, **97**, 187401.

52 A. P. Defante, T. N. Burai, M. L. Becker and A. Dhinojwala, *Langmuir*, 2015, **31**, 2398–2406.

53 S. Dalvi, A. Gujrati, S. R. Khanal, L. Pastewka, A. Dhinojwala and T. D. B. Jacobs, *Proc. Natl. Acad. Sci. U.S.A.*, 2019, **116**, 25484–25490.

54 T. Ohto, H. Tada and Y. Nagata, *Phys. Chem. Chem. Phys.*, 2018, **20**, 12979–12985.

55 K. Nanjundiah, P. Y. Hsu and A. Dhinojwala, *J. Chem. Phys.*, 2009, **130**, 024702.

56 M. K. Chaudhury, T. Weaver, C. Y. Hui and E. J. Kramer, *J. Appl. Phys.*, 1996, **80**, 30–37.

57 M. K. Chaudhury and G. M. Whitesides, *Langmuir*, 1991, **7**, 1013–1025.

58 G.-Y. Choi, J. F. Kang, A. Ulman, W. Zurawsky and C. Fleischer, *Langmuir*, 1999, **15**, 8783–8786.

59 B. Yurdumakan, G. P. Harp, M. Tsige and A. Dhinojwala, *Langmuir*, 2005, **21**, 10316–10319.

60 F. M. Fowkes, *J. Adhes. Sci. Technol.*, 1987, **1**, 7–27.

61 A. N. Gent, *Langmuir*, 1996, **12**, 4492–4496.

62 S.-Y. Chen, Y. Kaufman, A. M. Schrader, D. Seo, D. W. Lee, S. H. Page, P. H. Koenig, S. Isaacs, Y. Gizaw and J. N. Israelachvili, *Langmuir*, 2017, **33**, 10041–10050.

63 C. Liu, Z. Yu, D. Neff, A. Zhamu and B. Z. Jang, *Nano lett.*, 2010, **10**, 4863–4868.

64 Y. Ohno, K. Maehashi, Y. Yamashiro and K. Matsumoto, *Nano lett.*, 2009, **9**, 3318–3322.

65 W. Wu, Z. Liu, L. A. Jauregui, Q. Yu, R. Pillai, H. Cao, J. Bao, Y. P. Chen and S.-S. Pei, *Sens. Actuators B Chem.*, 2010, **150**, 296–300.

66 Z. Li, A. Kozbial, N. Nioradze, D. Parobek, G. J. Shenoy, M. Salim, S. Amemiya, L. Li and H. Liu, *ACS Nano*, 2016, **10**, 349–359.

67 K. L. Johnson, K. Kendall and A. D. Roberts, *Proc. R. Soc. Lond. A*, 1971, **324**, 301–313.

68 J.-H. Zhao, T. Ryan, P. S. Ho, A. J. McKerrow and W.-Y. Shih, *J. Appl. Phys.*, 1999, **85**, 6421–6424.

69 J. F. D. Liljeblad and E. Tyrode, *J. Phys. Chem. C*, 2012, **116**, 22893–22903.

70 A. G. Lambert, P. B. Davies and D. J. Neivandt, *Appl. Spectrosc. Rev.*, 2005, **40**, 103–145.